A Two-Electron Silver Superatom Isolated from Thermally Induced Internal Redox Reactions of A Silver(I) Hydride

Yu-Jie Zhong, Jian-Hong Liao, Tzu-Hao Chiu, Samia Kahlal, Che-Jen Lin, Jean-Yves Saillard, Chen-Wei Liu

10.1002/ange.202100965

WILEY-VCH

COMMUNICATION

A Two-Electron Silver Superatom Isolated from Thermally Induced Internal Redox Reaction of A Silver(I) Hydride

Yu-Jie Zhong,[a] Jian-Hong Liao,[a] Tzu-Hao Chiu,[a] Samia Kahlal,[b] Che-Jen Lin,[a] Jean-Yves Saillard*[b] and C. W. Liu*[a]

[a] Y.-J. Zhong, Dr. J.-H. Liao, T.-H. Chiu, Prof. Dr. Che-Jen Lin, Prof. Dr. C. W. Liu
Department of Chemistry
National Dong Hua University
No. 1, Sec. 2, Da Hsueh Rd., Hualien 974301, Taiwan (R.O.C.)
E-mail: chenwei@mail.ndhu.edu.tw
Homepage: http://faculty.ndhu.edu.tw/~cwl/index.htm

[b] Dr. S. Kahlal, Prof. Dr. J.-Y. Saillard
Univ Rennes, CNRS, ISCR-UMR 6226
F-35000 Rennes, France
E-mail: jean-yves.saillard@univ-rennes1.fr

Supporting information (experimental and computational details) of this article can be found under https://doi.org/10.1002/anie.xxxxxxxxx.

Abstract: Rational syntheses under controllable reducing conditions in the preparation of superatoms with cluster electron not exceeding two are challenging. Herein a dithiolate-stabilized two-electron silver nanocluster, $Ag_{10}\{S_2P(O^iPr)_2\}_8$ (**1**), is isolated via a self-redox reaction of $Ag_7(H)\{S_2P(O^iPr)_2\}_6$ without adding extra reducing agents. The metal framework of Ag_7, a bicapped trigonal bipyramid, is highly correlated to that of Ag_{10}, suggesting $Ag_7(H)\{S_2P(O^iPr)_2\}_6$ acts as both reducing agent and template in cluster growth. **1** is highly fluorescent at ambient temperature and TD-DFT calculations indicate that the emission is of $1P_x \rightarrow 1S$ nature.

The chemistry of atomically and structurally precise nanoclusters (NCs) has undergone a renaissance over the past few years owing to their numerous properties.[1] The stability and structure of NCs can often be rationalized within the concept of superatom and its "*magic*" closed-shell electron counts of 2, 8, 18, 20, 34, 40, 58...[2] Whereas the majority of reported silver superatoms are 8-electron species,[3] examples of 2-electron superatoms are surprisingly fewer (Table S1).[4-10] The first one, $Ag_{14}(SC_6H_3F_2)_{12}(PPh_3)_8$, was published in 2013.[4] It was followed in the same year by $[Ag_6(\gamma\text{-}H_2SiW_{10}O_{36})_2]^{8-}$,[5] and $Ag_{16}(dppe)_4(SC_6H_3F_2)_{14}$.[6] Additional 2-electron Ag NCs were reported only recently, thus becoming a hot topic in the NC community.[7-10] Most of the 2-electron Ag NCs listed in Table S1 have an octahedral $[Ag_6]^{4+}$ superatomic core, and the other silver atoms of the cluster, if any, are formally Ag(I).[4-5,7] The tetracapped tetrahedral $[Ag_8]^{6+}$ core is also well represented.[7e] Other examples display rhombohedral $[Ag_8]^{6+}$,[10] fcc-packed $[Ag_7]^{5+}$,[8] or anti-cuboctahedral $[Ag_{13}]^{11+}$ [9] cores. Most of them are co-protected by two or more types of ligands such as phosphines, thiolates, alkynyls, or polyoxometalates.[4-9] So far, only one homoleptic two-electron NC, $[Ag_8(pfga)_6]^{6-}$, is known.[10] In the present contribution, we report the isolation of a homoleptic, dithiolate-stabilized Ag_{10} 2-electron NC whose metal core is totally different from the above mentioned structures. Whereas most of the above-mentioned 2-electron species were prepared with borohydride,[4,6,9] silane,[5] or DMF[7,10] as reducing agents (Table S1), controlling the amount of reductants used in their synthesis to avoid the formation of 8-electron species can be problematic. Herein we describe an unprecedented controllable synthesis of a new 2-electron NC without additions of any reducing agent, that is, starting from a pre-organized silver(I) hydride compound as a both reducing agent and template. To the best of our knowledge, it is the first example of a thermally induced internal redox reaction of silver(I) hydride leading to the formation of a superatomic NC.

We have observed that the $Ag_7(H)\{S_2P(O^iPr)_2\}_6$[11] solution gradually changes color from transparent to light purple at ambient temperature, and then exhibits red emission under UV irradiation. However, this color change takes a long time. To speed up the process, the temperature was elevated to 60˚C. The experiment was carried out in a sealed NMR tube containing only $Ag_7(H)\{S_2P(O^iPr)_2\}_6$ and $CDCl_3$. Time-dependent $^{31}P\{^1H\}$ (Figure 1a) and ^1H (Figure 1b) NMR spectra were acquired from 0 to 72 hours. Almost no change occurred during the first three hours and a pseudo octet of octets coupling of hydride and silver nuclei was clearly seen in the ^1H NMR spectrum. After six hours, a peak centered at 104.5 ppm appeared in the $^{31}P\{^1H\}$ NMR spectrum, assignable to a new compound **1**, identified later as $Ag_{10}\{S_2P(O^iPr)_2\}_8$ (vide infra) and in-situ generated H_2 gas was identified at 4.6 ppm in the ^1H NMR spectrum. As the reaction continues, the intensities of the peak at 104.5 ppm and that of a new broad peak at 106.5 ppm increase. After 72 hours, the hydride resonance had completely disappeared, indicating that the $Ag_7(H)\{S_2P(O^iPr)_2\}_6$ reactant was completely consumed. The residual products are **1** and the species resonating at 106.5 ppm

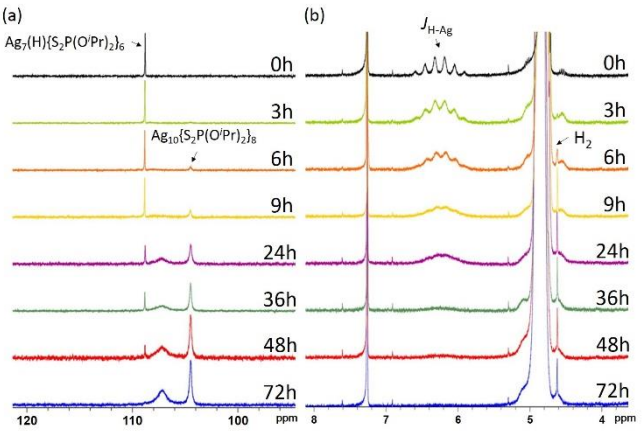

Figure 1. (a) Time-dependent $^{31}P\{^1H\}$ and (b) ^1H NMR spectra of **1**, recorded in a sealed NMR tube.

10.1002/ange.202100965

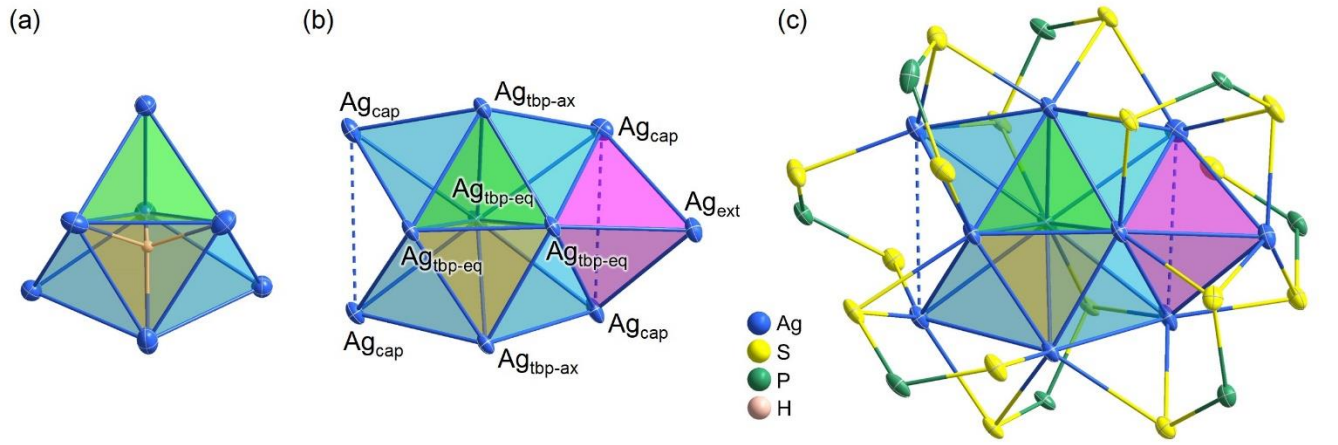

Figure 2. (a) A schematic representation of $Ag_7(H)$ core, and (b) Ag_{10} core in **1**. (c) The total structure of $[Ag_{10}\{S_2P(O^iPr)_2\}_8]$ with isopropoxy groups omitted for clarity.

in the ^{31}P NMR spectrum, which was identified as the $[Ag\{S_2P(O^iPr)_2\}]_n$ polymer (see below). The balanced reaction equation (Scheme 1) describes a self-redox process. We suggest that the encapsulated hydride of $Ag_7(H)\{S_2P(O^iPr)_2\}_6$ partly reduces the cluster silver(I) atoms, eventually yielding the 2-electron superatom **1**, concomitantly with the hydride oxidation in H_2.

$$2[Ag_7(H)\{S_2P(O^iPr)_2\}_6] \xrightarrow[THF]{60^oC} [Ag_{10}\{S_2P(O^iPr)_2\}_8] + 4/n\,[Ag\{S_2P(O^iPr)_2\}]_n + H_2$$

Scheme 1. The internal redox reaction of $Ag_7(H)\{S_2P(O^iPr)_2\}_6$.

Unfortunately, the slow transformation process at high temperature also favors decomposition. As a result, the highest yields possible reach ~42%. An alternative reaction was performed by adding 0.5 equivalent of $[Ag\{S_2P(O^iPr)_2\}]_6$[12] to an $Ag_7(H)\{S_2P(O^iPr)_2\}_6$ solution, then kept stirring at 60˚C (Figure S1, Scheme S2). Compound **1** can be formed in larger quantities within three hours, compared to the self-redox reaction of Scheme 1. H_2 is clearly detected in the ^1H NMR spectrum (Figure S2). As a result, the yield of **1** increases to ~53% after 24 hours, but starts to decrease for longer periods due to thermal instability of **1**. It can be assumed that when the self-redox reaction of $Ag_7(H)\{S_2P(O^iPr)_2\}_6$ occurs, the presence of $[Ag\{S_2P(O^iPr)_2\}]_6$ (Scheme S2) provides the building materials to speed up the formation of **1**. Nevertheless, the thermally induced internal redox reaction of $Ag_7(H)\{S_2P(O^iPr)_2\}_6$ discussed here is reminiscent of the degradation of the Cu(I) hydride $[Cu_{15}(H)_2(dtc)_6(C_2Ph)_6]^+$ (dtc = dithiocarbamate) into the 2-electon superatom $[Cu_{13}(dtc)_6(C_2Ph)_4]^+$. The latter was proposed to be generated from the former via sequential loss of $[CuC_2Ph]$ and H_2 formation.[13]

Interestingly, the X-ray structure of **1**[14] exhibits a metal framework that is closely related to that of its precursor $Ag_7(H)\{S_2P(OEt)_2\}_6$.[11] The $Ag_7(H)$ core of the latter can be viewed as a bicapped trigonal bipyramid (Figure 2a) with an encapsulated hydride lying in the yellow tetrahedron. The Ag_{10} metal framework in **1** (Figure 2b) contains the bicapped trigonal bipyramid of Ag_7 core, and additionally possesses two supplementary Ag atoms (Ag_{cap}) that cap the bipyramid. The resulting tetracapped trigonal bipyramid is further capped by an outer atom (Ag_{ext}), which connects two Ag_{cap} and one of the bipyramid equatorial atoms (Ag_{tbp-eq}), as illustrated in Figure 2b. In the structure of **1** (Table S2), the edge distances of the yellow tetrahedron (2.7985(13)-2.9567(13) Å, avg. 2.8562(13) Å) are similar to those in green tetrahedron (2.7848(14)-2.9192(13) Å, avg. 2.8553(13) Å). This is not the case for $Ag_7(H)\{S_2P(OEt)_2\}_6$ in which the edges of the hydride-containing yellow tetrahedron (3.149(3)-3.161(3) Å, avg. 3.155(3) Å) are significantly larger than those in the green tetrahedron (2.939(3)-3.161(3) Å, avg. 3.050(3) Å).[11] Thus, the equivalency between the yellow and green tetrahedra in **1** is consistent with the absence of hydride encapsulation. The four cyan tetrahedra in **1** are similar, with average edges (2.9495(13) Å) slightly larger than those of the bipyramid. The magenta tetrahedron is the largest, with average edges of 3.150(1) Å. Overall, both $Ag_7(H)\{S_2P(OEt)_2\}_6$ and **1** contain a similar bicapped trigonal bipyramidal metal core, strongly suggesting that the former behaves as a template to generate the latter.

The Ag_{10} framework of **1** is surrounded by eight dithiophosphate ligands (Figure 2c) in three coordination modes: one in bimetallic biconnectivity (μ_2: (η^1, η^1)), three in trimetallic triconnectivity (μ_3: (η^1, η^2)), and four in tetrametallic tetraconnectivity (μ_4: (η^2, η^2)).[15] Discarding the Ag-Ag contacts, all the Ag atoms are tri-coordinated (AgS_3), but the three $Ag_{tbp-eq.}$ which are bi-coordinated (AgS_2). The room-temperature $^{31}P\{^1H\}$ NMR spectrum reveals eight ligands in two environments (105.4 and 104.5 ppm) with the integration ratio of ~ 1:7 (Figure S3). The 293K-213K VT $^{31}P\{^1H\}$ NMR spectra (Figure S5) display slightly broadened peaks at 213K, indicating that all coordination environments are not discernible due to fluxional behavior in solution, even at low temperature. Presumably, the small peak at 105.4 ppm can be inferred to the unique ligand in bimetallic (η^1, η^1) connectivity.

The positive-mode ESI mass spectrum of **1** (Figure 3a) shows a molecular ion peak at m/z 2892.0670 corresponding to the intact neutral cluster with an additional silver ion, $[\mathbf{1} + Ag^+]^+$ (calc. m/z 2892.0923). The compound resonating at 106.5 ppm in the ^{31}P NMR spectrum was separated by chromatography and its positive-mode ESI mass spectrum displayed an enveloped distribution corresponding to $[Ag_n\{S_2P(O^iPr)_2\}_n + Ag^+]^+$, n = 3-10 (Figure S6, Table S3), indicative of a $[Ag\{S_2P(O^iPr)_2\}]_n$ polymer.

The UV-vis absorption spectrum (Figure 3b) of **1** in 2-MeTHF shows two prominent bands at 348 nm (ε = 15500 M^{-1} cm^{-1}), 392 nm (ε = 21300 M^{-1} cm^{-1}), and a characteristic peak at 520 nm (ε = 8100 M^{-1} cm^{-1}). Compound **1** shows red emission under UV irradiation at ambient temperature, in both solid state (725 nm)

10.1002/ange.202100965

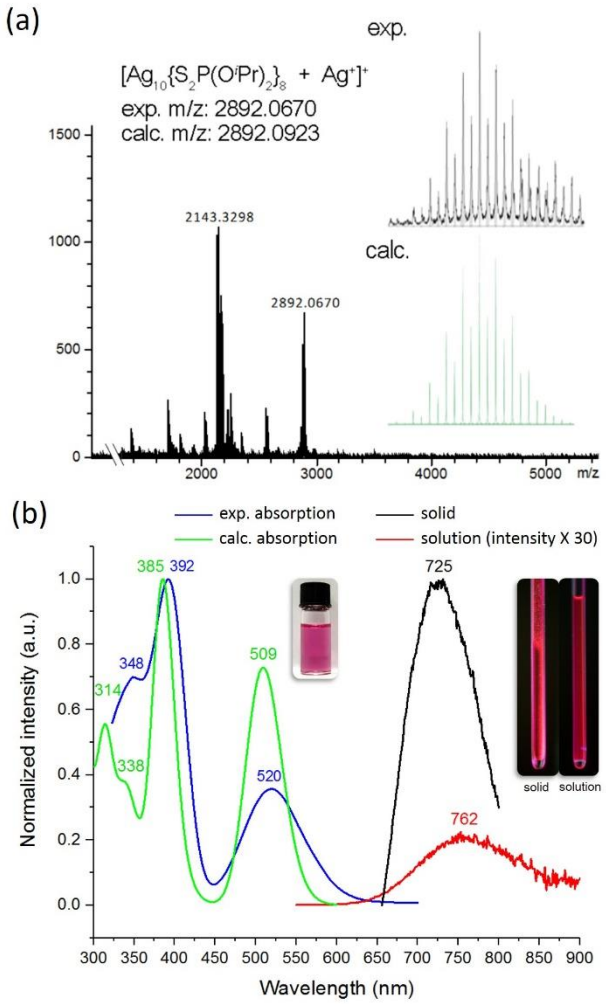

Figure 3. (a) The positive-mode ESI mass spectrum of **1**, the inset spectra are experimental (top) and calculated (bottom) isotopic distribution pattern of $[Ag_{10}\{S_2P(O^iPr)_2\}_8 + Ag^+]^+$. (b) Experimental (blue), calculated (green) absorption, and emission spectra of **1** in solid (black) and 2-MeTHF (red) at ambient temperature. The intensity of **1** in 2-MeTHF is increased by 30 times for comparison. The inset pictures are the compound **1** (left) in 2-MeTHF, and **1** in solid and 2-MeTHF irradiated under UV light (right).

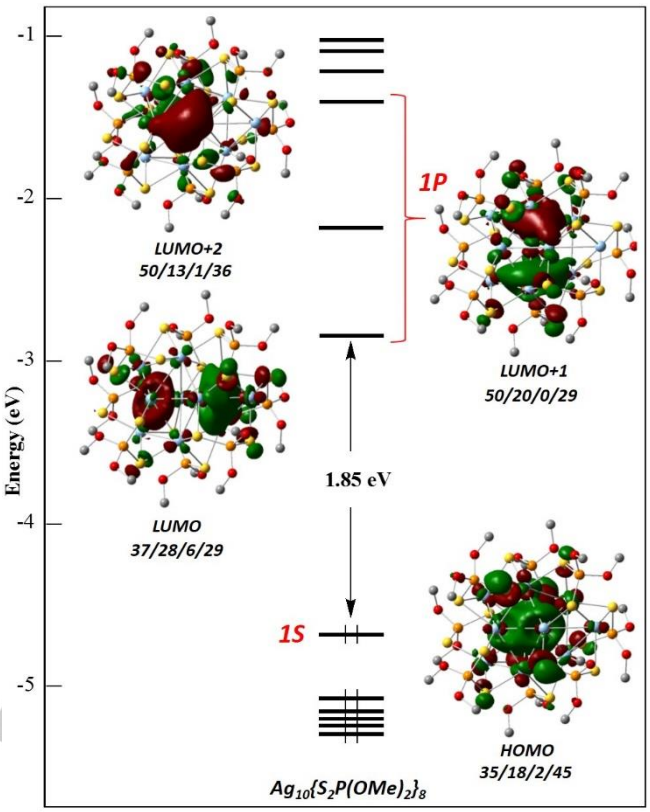

Figure 4. Kohn-Sham orbital diagram of **1'**. The MO localizations (in %) are given in the following order: $(Ag_{tbp})_5/(Ag_{cap})_4/Ag_{ext}$/ligands.

and solution (762 nm), and the emission intensity in solid state is ~150 times stronger than that in solution (QY = 6.0%). A pronounced emission blue-shift occurs at 77K (Figure S7) in both solid (693 nm) and 2-MeTHF glass (687 nm). In contrast to **1**, $[Ag_7(H)\{S_2P(O^iPr)_2\}_6$ shows very weak yellow emission at 77K. The stability of **1** can be determined by time-dependent UV-vis absorption spectra. The absorption profiles do not change in dark over 14 days (Figure S8a), but gradually decreases under day light in 6 days (Figure S8b). The photoluminescence (PL) lifetime of **1** in 2-MeTHF recorded at room temperature (Figure S9) is 2.0 ns (96.5 %) and 7.3 ns (3.5 %), which differs significantly from the lifetime (0.4 ns, 47.3%; 7.0 ns, 52.7%) in solid state at RT (Figure S11). It demonstrated longer lifetime in both frozen glass (0.1 ns, 9.4%; 15.4 ns, 90.6%) and solid (0.6 ns, 7.6%; 12.9 ns, 92.6%) at 77K. This can be attributed to the hampering of molecular motion in the condensed phases, which reduces non-radioactive decay. In any event, the recorded lifetimes are consistent with a fluorescence behavior. Photophysical data of **1** are summarized in Table S4.

DFT calculations (see SI for details) were performed at the BP86-D3/Def2-TZVP level on the simplified model $Ag_{10}\{S_2P(OMe)_2\}_8$ (**1'**). Its optimized geometry, characterized as an energy minimum, matches quite well with the X-ray structure of **1** (Table S2), with a overestimation by ~ 3% of the Ag-Ag contacts, as expected at this level of theory. Its Kohn-Sham orbital diagram (Figure 4) exhibits a substantial energy gap of 1.85 eV. The HOMO lies 0.38 eV above the HOMO-1. It can be identified as the 1S superatomic orbital, with significant ligand admixture. It has a 35% contribution from the trigonal bypyramid (with almost equal participation of the five atoms). The four Ag_{cap} participate to a total of 18%, whereas that of Ag_{ext} is only 2%. The three lowest vacant MOs can be viewed as the split 1P shell and their ligand contribution is modest. The averaged metal natural atomic orbital (NAO) charges range 0.32 ($Ag_{tbp\text{-}eq}$), 0.62 ($Ag_{tbp\text{-}ax}$), 0.68 (Ag_{cap}) and 0.76 (Ag_{ext}). The Wiberg bond indices (Table S5) indicate significant $Ag_{tbp\text{-}eq}$-$Ag_{tbp\text{-}eq}$ bonding, whereas the Ag_{cap} and Ag_{ext} atoms are mainly involved in metallophillic-like interactions. Taken all together, these results suggest that the two superatomic electrons are mainly localized on the trigonal bipyramid and mainly on its equatorial triangle. The TD-DFT-simulated UV-vis spectrum of **1'** is shown in Figure 3b. It reproduces nicely the experimental spectrum. The band at 509 nm corresponds to a HOMO (1S) → LUMO ($1P_x$) transition and that at 385 is mainly of HOMO (1S) → LUMO+1 ($1P_z$) character. The band of higher energy is split into two components (338 and 314 nm), which are a mixture of the HOMO (1S) → LUMO+2 ($1P_y$) and various ligand → metal transitions. An estimated S1 → S0 emission wavelength, calculated by TD-DFT yielded a value of 688 nm, corresponding to a $1P_x$ → 1S transition.

In conclusion, a new methodology is developed to prepare superatomic nanoclusters in a controllable fashion. $Ag_7(H)\{S_2P(O^iPr)_2\}_6$ in solution proceeds self-redox reactions to yield H_2 and a new 2-electron silver superatom, $Ag_{10}\{S_2P(O^iPr)_2\}_8$ of unique trigonal bipyramidal core structure. The transformation is triggered by visible light in slow speed or boosted by heating. Both $Ag_7(H)$ and Ag_{10} cores have a similar trigonal bipyramidal-based skeleton, indicating that $Ag_7(H)\{S_2P(O^iPr)_2\}_6$ plays dual roles: a reducing agent and a template for cluster growth. $Ag_{10}\{S_2P(O^iPr)_2\}_8$ exhibits strong red emission at ambient temperature in solution with quantum yield of 6.0%. We hope this work, which uses a hydrido silver(I) cluster without adding extra reducing agents, can provide a new concept for synthesizing superatomic NCs. This work also provides a solid experimental proof that a hydrido silver(I) complex is a key component for the growth of superatoms even though they have been proposed in several occasions.[16] It is anticipated those structurally characterized group 11 hydride clusters,[17] if thermally stable, may eventually reach the stage of higher electron-count superatoms by applying this methodology.

Acknowledgements

This work was supported by the Ministry of Science and Technology of Taiwan (MOST 109-2113-M-259-008, 108-2923-M-259-001), and the France-Taiwan ANR-MOST program (project Nanoalloys). The GENCI (Grand Equipment National de Calcul Intensif) is acknowledged for HPC resources (Project A0050807367).

Conflict of interest

The authors declare no conflict of interest.

Keywords: superatom • silver nanocluster • redox • silver • hydride

[1] a) S. Maity, D. Bain, A. Patra, *Nanoscale* **2019**, *11*, 22685-22723; b) Y. Du, H. Sheng, D. Astruc, M. Zhu, *Chem. Rev.* **2020**, *120*, 526-622; c) X. Kang, M. Zhu, *Chem. Soc. Rev.* **2019**, *48*, 2422-2457; d) R. Jin, C. Zeng, M. Zhou, Y. Chen, *Chem. Rev.* **2016**, *116*, 10346-10413.

[2] a) M. Walter, J. Akola, O. Lopez-Acevedo, P. D. Jadzinsky, G. Calero, C. J. Ackerson, R. L. Whetten, H. Grönbeck, H. Häkkinen, *Proc. Natl. Acad. Sci. U.S.A.* **2008**, *105*, 9157-9162; b) H. Häkkinen, *Chem. Soc. Rev.* **2008**, *37*, 1847-1859.

[3] a) R. S. Dhayal, J.-H. Liao, Y.-C. Liu, M.-H. Chiang, S. Kahlal, J.-Y. Saillard, C. W. Liu, *Angew. Chem. Int. Ed.* **2015**, *54*, 3702-3706; *Angew. Chem.* **2015**, *127*, 3773-3777; b) L. G. AbdulHalim, M. S. Bootharaju, Q. Tang, S. D. Gobbo, R. G. AbdulHalim, M. Eddaoudi, D.-e. Jiang, O. M. Bakr, *J. Am. Chem. Soc.* **2015**, *137*, 11970-11975; c) C. P. Joshi, M. S. Bootharaju, M. J. Alhilaly, O. M. Bakr, *J. Am. Chem. Soc.* **2015**, *137*, 11578-11581; d) R. S. Dhayal, Y.-R. Lin, J.-H. Liao, Y.-J. Chen, Y.-C. Liu, M.-H. Chiang, S. Kahlal, J.-Y. Saillard, C. W. Liu, *Chem. Eur. J.* **2016**, *22*, 9943-9947; e) Z.-J. Guan, J.-L. Zeng, Z.-A. Nan, X.-K. Wan, Y.-M. Lin, Q.-M. Wang, *Sci. Adv.* **2016**, *2*, e1600323; f) W.-T. Chang, P.-Y. Lee, J.-H. Liao, K. K. Chakrahari, S. Kahlal, Y.-C. Liu, M.-H. Chiang, J.-Y. Saillard, C. W. Liu, *Angew. Chem. Int. Ed.* **2017**, *56*, 10178-10182; *Angew. Chem.* **2017**, *129*, 10312-10316; g) X.-T. Shen, X.-L. Ma, Q.-L. Ni, M.-X. Ma, L.-C. Gui, C. Hou, R.-B. Hou, X.-J. Wang, *Nanoscale* **2017**, *10*, 515-519; h) X. Zou, S. Jin, W. Du, Y. Li, P. Li, S. Wang, M. Zhu, *Nanoscale* **2017**, *9*, 16800-16805; i) Z.-J. Guan, F. Hu, S.-F. Yuan, Z.-A. Nan, Y.-M. Lin, Q.-M. Wang, *Chem. Sci.* **2019**, *10*, 3360-3365; j) T. Omoda, S. Takano, T. Tsukuda, *Small* **2021**, DOI: 10.1002/smll.202001439.

[4] H. Yang, J. Lei, B. Wu, Y. Wang, M. Zhou, A. Xia, L. Zheng, N. Zheng, *Chem. Commun.* **2013**, *49*, 300-302.

[5] Y. Kikukawa, Y. Kuroda, K. Suzuki, M. Hibino, K. Yamaguchi, N. Mizuno, *Chem. Commun.* **2013**, *49*, 376-378.

[6] H. Yang, Y. Wang, N. Zheng, *Nanoscale* **2013**, *5*, 2674-2677.

[7] a) Z.-Y. Wang, M.-Q. Wang, Y.-L. Li, P. Luo, T.-T. Jia, R.-W. Huang, S.-Q. Zang, T. C. W. Mak, *J. Am. Chem. Soc.* **2018**, *140*, 1069-1076; b) Z. Wang, H.-F. Su, M. Kurmoo, C.-H. Tung, D. Sun, L.-S. Zheng, *Nat. Commun.* **2018**, *9*, 2094; c) Z. Wang, F.-L. Yang, Y. Yang, Q.-Y. Liu, D. Sun, *Chem. Commun.* **2019**, *55*, 10296-10299; d) Z. Wang, Q.-P. Qu, H.-F. Su, P. Huang, R. K. Gupta, Q.-Y. Liu, C.-H. Tung, D. Sun, L.-S. Zheng, *Sci. China Chem.* **2020**, *63*, 16-20; e) X.-M. Luo, C.-H. Gong, L. Zhang, S.-Q. Zang, *Nano Res.* **2020**, DOI: 10.1007/s12274-020-3227-5.

[8] K. Yonesato, H. Ito, D. Yokogawa, K. Yamaguchi, K. Suzuki, *Angew. Chem. Int. Ed.* **2020**, *59*, 16361-16365; *Angew. Chem.* **2020**, *132*, 16503-16507.

[9] S.-F. Yuan, P. Li, Q. Tang, X.-K. Wan, Z.-A. Nan, D.-e. Jiang, Q.-M. Wang, *Nanoscale* **2017**, *9*, 11405-11409.

[10] K.-G. Liu, X.-M. Gao, T. Liu, M.-L. Hu, D.-e. Jiang, *J. Am. Chem. Soc.* **2020**, *142*, 16905-16909.

[11] C. W. Liu, Y.-R. Lin, C.-S. Fang, C. Latouche, S. Kahlal, J.-Y. Saillard, *Inorg. Chem.* **2013**, *52*, 2070-2077.

[12] C. W. Liu, J. T. Pitts, J. P. Fackler Jr., *Polyhedron* **1997**, *16*, 3899-3909.

[13] K. K. Chakrahari, J. Liao, R. P. B. Silalahi, T.-H. Chiu, J.-H. Liao, X. Wang, S. Kahlal, J.-Y. Saillard, C. W. Liu, *Small* **2021**, DOI: 10.1002/smll.202002544.

[14] CCDC 2054938 contains the supplementary crystallographic data for compound **1** in this paper. This data can be obtained free of charge from The Cambridge Crystallographic Data Centre via www.ccdc.cam.ac.uk/data_request/cif.

[15] I. Haiduc, L. Y. Goh, *Coord. Chem. Rev.* **2002**, *224*, 151-170.

[16] S, Sharma, K. K. Chakrahari, J.-Y. Saillard, C. W. Liu, *Acc. Chem. Res.* **2018**, *51*, 2475-2483.

[17] a) R. S. Dhayal, W. E. van Zyl, C. W. Liu, *Acc. Chem. Res.* **2016**, *49*, 86-95; b) T. Nakajima, K. Nakamae, Y. Ura, T. Tanase, *Eur. J. Inorg. Chem.* **2020**, 2011-2226; c) C. Sun, B. K. Teo, C. Deng, J. Lin, G.-G. Luo, C.-H. Tung, D. Sun, *Coord. Chem. Rev.* **2021**, *427*, 213576.

10.1002/ange.202100965

WILEY-VCH

COMMUNICATION

Entry for the Table of Contents

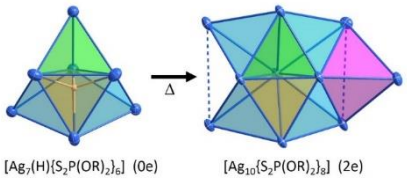

A self-redox reaction of $Ag_7(H)\{S_2P(O^iPr)_2\}_6$ leads to the formation of a highly emissive, two-electron Ag nanocluster, $Ag_{10}\{S_2P(O^iPr)_2\}_8$, without adding extra reducing agents. The metal framework of Ag_7, a bicapped trigonal bipyramid, is highly correlated to that of Ag_{10}, suggesting $Ag_7(H)\{S_2P(O^iPr)_2\}_6$ acts as both reducing agent and template in cluster growth.